Memoirs of the Faculty of Engineering and Design
Kyoto Institute of Technology 50 (March, 2002)

Control of RFP Dynamics Using External Helical Fields

Sadao MASAMUNE and Motomi IIDA

(Received September 3, 2001; Accepted September 3, 2001)

Abstract

Control of the MHD mode dynamics is essential to improving reversed field pinch (RFP) experiments as a part of the fusion research programs. Influence of the static and rotating helical fields on the RFP dynamics has been studied in the STE-2 RFP to test the idea of the use of helical field for the control of MHD modes. Emphasis is put on the resistive wall modes which play important roles in future RFPs where plasma lifetime is much longer than the field penetration time of the wall. Static resonant helical field brings about unfavorable effect, as expected, by enhancing the magnetic islands, while rotating resonant field is shown to be a possibile tool for the control of tearing mode dynamics. The effect of externally nonresonant field on external kink modes is also discussed.

Key Words: *reversed field pinch; MHD relaxation; mode dynamics; external helical field; resistive wall mode;*

1. Introduction

The reversed field pinch (RFP) is characterized by the magnetohydrodynamic (MHD) relaxation to attain a near minimum energy configuration and subsequent dynamo activities for sustaining the configuration. It has been established that m(poloidal mode number)=1 internal tearing modes (resonant inside the field reversal surface) and/or internal kink modes play an essential role in the dynamics of the MHD relaxation and dynamo.[1),2)] On the other hand, nonlinear coupling of these instabilities, or, overlapping of the magnetic islands associated with these modes, has been believed to result in stochastic field lines in the core region, causing magnetic fluctuation-induced transport to be dominant in the RFP.[3),4)] A dramatic improvement of the confinement has been demonstrated recently by the reduction of magnetic fluctuation associated with core resonant tearing modes utilizing the technique of current profile control.[5)] A new operation regime of improved confinement has also been explored by carefully adjusting the waveforms of the plasma current and toroidal magnetic flux to minimize the dynamo activity together with sufficient wall conditioning.[6)]

The unfavorable aspects of the MHD instabilities are more pronounced in the RFP with resistive boundary,[7–12)] where RFP discharge duration (τ_d) is comparable to or longer than shell time constant (τ_s). In these circumstances, stability boundary of the tearing modes is affected by τ_s and the distance to the shell as well.[13),14)] Toroidal rotation of the plasma with

sufficient velocity is shown to have a stabilizing effect on the resistive modes in resistive boundary RFP.[13),14)] Feedback stabilization[15)] may not be applicable in the RFP where many modes with different helicities have to be stabilized simultaneously. Ideal external kink modes can also be unstable[12)] in the timescale of τ_s, however, these modes have been shown to be stabilized with feedback control.[16)]

Development of an effective means to stabilize the tearing modes in resistive boundary is thus one of the important issues in the RFP research. The present work has been motivated by our interest in the possibility of driving plasma rotation using a toroidally rotating resonant helical field. The rotation would be driven if the net accelerating torque could be generated by the interaction between the inherent tearing mode and suitably phased rotating resonant helical field.[17),18)] Study on interaction of the RFP plasma with external helical fields is thus quite important. However, as far as our knowledge is concerned, no systematic study has been made to date. In this regard, we should note that in the OHTE[19),20)] experiment, now modified to the Extrap T2 expermiment,[12)] it has been demonstrated that the pitch reversal (RFP configuration) could be produced and sustained inside a separatrix by external helical windings, without toroidal field coils. Although the OHTE applied much stronger fields than our present experiment, they might be similar to each other in that the helical pitch of the magnetic field is influenced by the external windings in the outer region.

In this paper, recent results on the MHD mode dynamics under the influence of external helical field are summarized. First, the RFP plasma response to four kinds of external static helical fields having different helicities[21)] is described. A stability analysis on resistive wall kink mode which was motivated by the experiment will follow, and, finally, studies on mode dynamics using rotating helical fields (RHFs) are described.

2. Experimental Arrangement

The STE-2[22)] is a small-size RFP machine ($R/a=0.4\text{m}/0.1\text{m}$) in which we used a 2 mm thick SS chamber, where R is the major radius and a, the minor radius. The time constant of the chamber for the vertical field penetration, $\tau_c=\mu_0 ad/2\eta_c$, was 0.25 ms, where d is the chamber thickness, μ_0 the vacuum permeability, and η_c the chamber resistivity.

In the static perturbation experiments, the chamber was covered by a close fitting 0.5 mm thick copper shell with the minor radius b of 0.103 m. The shell time constant was 1.7 ms, and the combined time constant 2 ms, twice as long as typical discharge duration in our experiment. In the RHF experiments the shell was removed, the vacuum vessel working as a resistive wall.

Twelve turn primary windings were set coaxially with the chamber outside the shell at $r_{pr}=0.115$ m. Four kinds of helical windings were attached at $r_{he}=0.121$ m, slightly outside the primary windings. These helical windings produced perturbation fields with $\text{M/N}=1/\pm 8$ and $1/\pm 10$, where M and N are the poloidal and toroidal mode numbers of the perturbation field, respectively. Hereafter we will use m and n to designate the mode numbers of the inherent magnetic fluctuations.

Internal magnetic field profile measurements showed that, in a typical RFP discharge

which was slightly degraded by insertion of magnetic probes to the magnetic axis, the safety factor q was about 0.15 on the axis, decreasing to ~-0.03 at the edge. The M/N=1/8 perturbation was resonant at $r/a=0.4$, and the 1/10 at $r/a=0.5$. These perturbations will be referred to as internally resonant, or, resonant for short. The perturbation fields with negative N had no resonance between the field reversal surface and the shell, so that they will be referred to as (externally) nonresonant.

The amplitude of external field at the edge is denoted by $|B_{ra}|$, and $|B_{ra}|/B_{\theta a}$ will be referred to as the external perturbation level, where $B_{\theta a}$ is the edge poloidal field at the peak plasma current.

The major diagnostics were magnetic pickup coils and flux loops. An array of toroidal flux loops were used to study toroidal flux disturbance localized near the poloidal gap. In addition, a calorimeter probe was used for the measurement of edge heat flux most of which were shown to be carried by the superthermal electrons.

3. RFP Plasma Response to Static Helical Fields

Figure 1 shows time traces of discharges with and without the helical perturbations. When the nonresonant perturbations were applied, as shown in Fig.1(a), the RFP discharges were improved slightly, where the improvement resulted mainly from reduced discharge resistance. The improvement was observed for the perturbation level of up to ~8 %.

When the resonant perturbations were applied, the RFP discharges resulted in degradation with decreased plasma current, higher loop voltage and shorter discharge duration, as shown in Fig.1(b). The degradation is evident with the level of 1 %, which is slightly higher than the inherent fluctuation level, $|\tilde{B}_{ra}|/B_{\theta a}$, associated with the m=1 tearing modes when compared at the edge, where $|\tilde{B}_{ra}|$ is the root-mean-square inherent fluctuation amplitude.

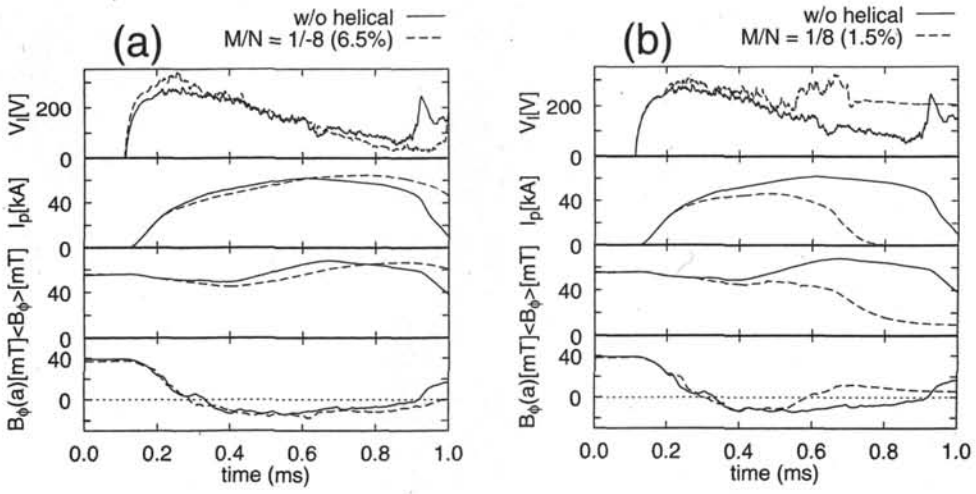

Fig.1 Time traces of the loop voltage V_l, plasma current I_p, average $<B_\phi>$ and edge $B_{\phi a}$ toroidal fields in RFP discharges (a)with externally nonresonant (6.5 % M/N=1/-8) perturbation and (b)with internally resonant (1.5 % M/N=1/8) static helical field, compared with those without perturbations.

Dependence of the discharge resistance on the amplitude of the helical perturbations are summarized in Fig.2(a) for the nonresonant perturbations and in Fig.2(b) for the resonant ones. It should be noted that the comparison has been made under the same conditions of the power supplies (charging voltage of the poloidal and toroidal circuits) as well as fill pressure of the working gas (hydrogen). The peak plasma current does not increase significantly with application of the nonresonant perturbations, so, the decreased resitance is brought about mainly by decreased loop voltage, in the average sense. While, on the other hand, the discharge resistance increased with resonant perturbations of only 1 % level. It became difficult for the peak plasma current to exceed 50 kA for the M/N=1/8 perturbation of the level of higher than 2 %. The RFP configuration could not be sustained for the periods longer than ~0.2 ms in these degraded discharges. It should be noted that the critical amplitude for the degradation to such a degree increased by about a factor 2 (amplitude of about 4 %) for M/N=1/10 perturbations whose resonant surface was located radially outside of the 1/8 resonance by about 1 cm ($0.1a$).

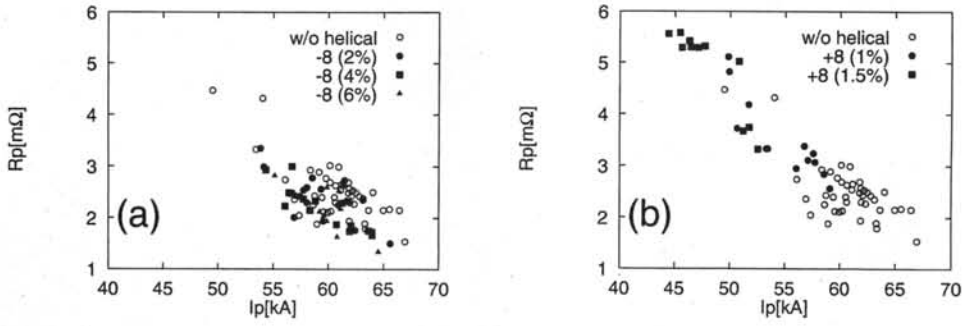

Fig.2 Discharge resistance V_l/I_p vs. maximum I_p in RFP discharges with (a)nonresonant and (b)resonant helical fields.

In Fig.3(a) (with M/N=1/±8 perturbations) and Fig.3(b) (with 1/±10 perturbations), the $F-\Theta$ loci at the time of maximum plasma current are comparatively shown with nonresonant (open rectangles), resonant (filled rectangles), and without perturbations (open circles). Here $F(=B_{\phi a}/<B_\phi>)$ is the field reversal ratio and $\Theta(=B_{\theta a}/<B_\phi>)$, the pinch parameter, where $B_{\phi a}$ is the edge toroidal field and $<B_\phi>$ the average toroidal field. It should be noted that the conditions of the power supplies as well as the fill pressure remained fixed in the comparison.

The Θ values tend to scatter in the region of 1.8-2.4 without perturbations, the average

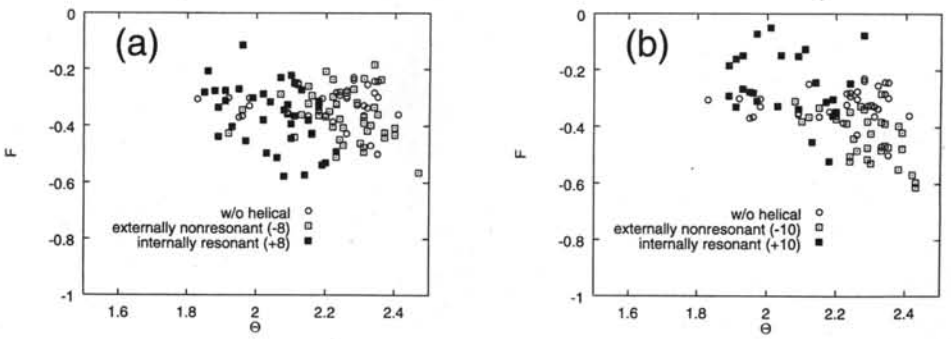

Fig.3 Comparison of the $F-\Theta$ location with (a)M/N=1/±8 and (b)M/N=1/±10 helical field.

value being around 2.2. The F values lie in the range from -0.3 to -0.4. The region of the Θ values is lower (with the average of ~2.0) with resonant perturbations, while it is higher (with the average ≥2.3) with nonresonant ones. The F values tend to scatter with 1/8 perturbations. With 1/10 perturbations, the region of the F values shows shallow reversal.

The observed tendency of the Θ value may be understood in connection with the RFP dynamo activity, which is essentially conversion of the poloidal magnetic flux into toroidal. Lower Θ is an indication of the higher rate flux conversion and higher Θ, the lower rate conversion, when compared under the same conditions of the power supplies.

It has been widely accepted that the RFP dynamo suppresses the parallel current in the core region while enhancing the poloidal (parallel) current at the edge, interaction of the internal m=1 tearing modes playing a major role in its dynamics.[23] Thus, the experimental lower Θ tendency is an indication of more active interaction of the m=1 modes. It is consistent with the observation that root-mean-square fluctuation level of the edge radial field increased with increasing the resonant perturbation; The incremental fluctuation level is about 50 % near the critical level for the degradation. The fluctuation level does not change significantly with nonresonant perturbations.

A direct comparison of the mode coupling process would require time evolution of the toroidal mode spectrum, which, however, is beyond the capability of our present diagnostics. Change of the coherence scale length, which is a measure of the spectral width resulting from mode coupling, will be discussed later.

In Fig.4, the toroidal magnetic flux in the different toroidal positions is shown, which were measured with 6 flux loops separated by 15° toroidally, where only the low frequency part (f<20 kHz) is shown. The suffix in the figure designates the location of the flux loop; ψ_1 is just at one of the poloidal gaps with suffix increasing in the opposite direction to the plasma current.

As shown in Fig.4(a), with resonant M/N=1/8 perturbations of 1 % amplitude, the initial increase of the flux starts almost uniformly at ~0.2 ms. The second flux increase, which starts at ~0.3 ms in ψ_2, appears to propagate toroidally with a velocity of ~6 km/s. Furthermore, the stop of the flux increase propagates with a reduced speed of ~4 km/s. The time evolution of ψ_1 is slightly different from that of the others, increasing to ~0.5 ms, after which the flux decreases at all the locations.

As is clear in Fig.4(b), with nonresonant 1/-8 perturbations of 4 % amplitude, toroidal uniformity in the flux behavior is greatly improved throughout a discharge. The

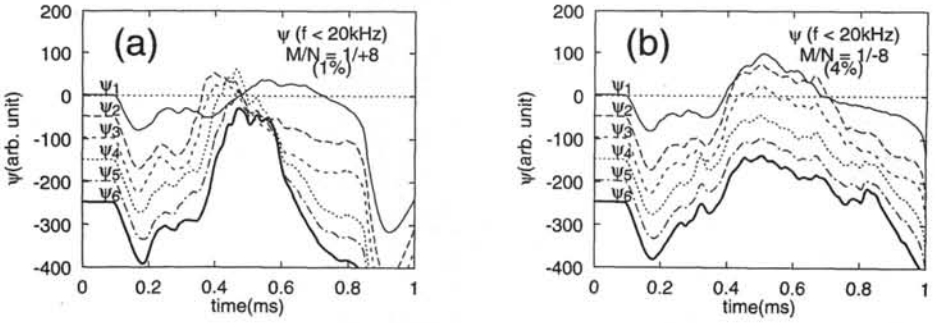

Fig.4 Time evolution of the toroidal magnetic flux at 6 toroidal locations separated by 15° toroidally. Only the low-frequency part (f<20 kHz) is shown with (a)resonant and (b)nonresonant helical field.

improvement of the toroidal uniformity appears to increase with an increase in the nonresonant perturbation amplitude of up to ~8 %. Thus the slightly improved discharge performance with nonresonant perturbations is accompanied by the improved toroidal uniformity of the toroidal flux.

Since the localized increase of the flux is a result of the phase locking of the m=0 modes resulting from nonlinear coupling of the modes, the above results suggest that the m=0 mode coupling is enhanced with application of resonant perturbations, while it is suppressed with nonresonant perturbations. The change in propagation velocity shown in Fig.4(a) might also suggest the relation of the resonant perturbation to the subsequent mode locking.

Correlation analysis of the magnetic fluctuations from the poloidal array inside the vessel revealed that magnetic fluctuations in the STE-2 were characterized by low frequency (f<50 kHz) m=0 component and high frequency (f ≥100 kHz) m=1 component. In Fig.5, coherence is plotted as a function of the poloidal length of separation of the two pickup coils. Here, coherence γ is related to the spectral width Δk as $\Delta k \propto (1-\gamma)^{1/2}$, which is a measure of the nonlinear mode coupling. Since the magnetic field at the RFP edge is mainly poloidal, the poloidal length may be regarded as the length along the mean magnetic field line in the approximate sense. The e-folding length of the coherence, which we will refer to as coherence scale length $\Lambda_{\parallel}$, is fairly long either without the perturbation or with nonresonant perturbations. When the resonant perturbations are applied, coherence decreases rapidly with poloidal length, $\Lambda_{\parallel}$ being comparable to the plasma minor radius. The decreased coherence is thus attributable to the enhanced nonlinear coupling of the internal m=1 tearing modes, being consistent with the lower Θ tendency described previously.

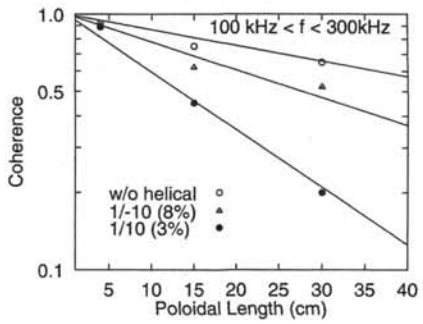

Fig.5 Coherence averaged over the m=1 frequency domain vs. poloidal length between the two pickup coils. The scale length decreases with resonant helical field.

It is worth comparing the results with coherence measurement in MST,[24] where change of coherence along the poloidal length was measured in several frequency domains. It was reported that the coherence scale length was fairly long in the frequency domain corresponding to the core resonant m=1 tearing modes. It is almost the same as the present results with nonresonant or without helical perturbations. The scale length decreased down to the order of plasma minor radius in the frequency domain corresponding to the turbulent fluctuations. The edge turbulence was attributed to the interaction of locally resonant m=1 modes whose resonant surfaces are closely spaced in the edge region. The decreased coherence scale length is similar to the present results with resonant helical fields. The comparison suggests that the m=1 mode coupling may be enhanced with the help of a static magnetic island due to the resonant helical field.

Static magnetic island widths produced by the resonant perturbations were estimated by

analyzing the following simple RFP equilibrium.[25] The analysis is an extension to the M=1 helical perturbation of the method by Pinsker and Reiman,[26] who treated the M=0 perturbed equilibria. In the present analysis, RFP equilibrium with uniform force-free parameter $\lambda(=j_{\parallel}/B)$ was adopted with a static M=1 helical field in an ideal shell with proximity b/a of 1.03.

In the cylindrical approximation, the helical flux function in the plasma $\psi_p(r,\theta,z)$ can be expressed as follows,

$$\psi_p(r,\theta,z) = \psi_{p0}(r) - A_N \psi_{p1}(r)\cos u_N, \tag{1}$$

$$\psi_{p0}(r) = (B_0/\lambda)[J_0(\lambda r) + k_N r J_1(\lambda r)], \tag{2}$$

$$\psi_{p1}(r) = \lambda J_1(\lambda_N r) - k_N \lambda_N r J'_1(\lambda_N r), \tag{3}$$

where J_0 and J_1 are the Bessel functions of the first kind, B_0 is the central magnetic field, $k_N = N/R$, $u_N = \theta - k_N z$, and $\lambda_N = (\lambda^2 - k_N^2)^{1/2}$. In the vacuum region, the helical flux function $\psi_v(r,\theta,z)$ can be expressed as follows,

$$\psi_v(r,\theta,z) = \psi_{v0}(r) - \psi_{v1}(r)\cos u_N, \tag{4}$$

$$\psi_{v0}(r) = C + (k_N r^2/2)B_T - aB_{\theta a} ln(r/a), \tag{5}$$

$$\psi_{v1}(r) = B_N k_N^2 r I'_1(k_N r) + C_N k_N^2 r[K'_1(k_N r) - \frac{K'_1(k_N b)}{I'_1(k_N b)} I'_1(k_N r)], \tag{6}$$

where I_1 and K_1 are the modified Bessel functions, B_T is the uniform vacuum toroidal field, and the coefficient B_N is related to the perturbation amplitude at the edge b_1 as $B_N = b_1/(k_N^2 I'_1(k_N a))$. C is a constant to be determined from the following matching condition. The perturbed plasma boundary ρ can be written as

$$\rho = a + A_N(\psi_{p1}(a)/\psi'_{p0}(a))\cos u_N. \tag{7}$$

Normal (ψ_p, ψ_v) and tangential ($\mathbf{n}\cdot\nabla\psi_p$, $\mathbf{n}\cdot\nabla\psi_v$) components of the magnetic fields were connected, respectively, at the perturbed plasma-vacuum boundary, where $\mathbf{n}$ is the surface normal vector. From these matching conditions, we could determine the coefficients, deriving the relation bewteen the magnetic island width and perturbation level.

Figure 6 shows the magnetic island width normalized to the plasma radius ($W/2a$) as a function of Θ for some values of the perturbation level. It shows that M/N=1/8 perturbation level of ~1 % produces an island with the width of ~10 % of the plasma minor radius, which approximately equals the radial separation of the neighboring rational surfaces in the core region. The perturbation level increases up to ~2 % for the M/N=1/10 perturbation to produce an island with the same width, mainly because of the higher magnetic shear at the corresponding resonant surface. In real RFP plasmas, λ decreases to 0 towards the edge. Radial variation of λ in the core region ($r/a \leq 0.5$), however, is not so large, and, therefore, the present results may apply, at least semi-quantitavely, to real RFP plasmas. The experimentally observed critical perturbation level for sustained RFP is therefore

attributable to sufficient overlapping of the static and inherent islands.

The discharge performance may be improved slightly with the nonresonant perturbations. Here we will discuss some possible mechanisms as further issues.

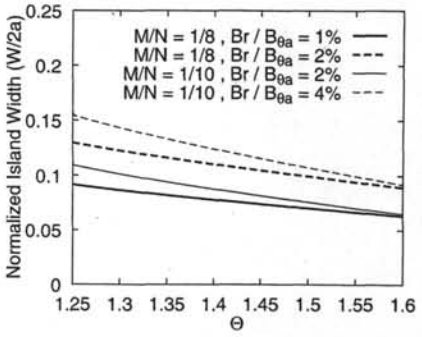

Fig.6 Magnetic island width W with M=1 helically perturbed RFP equilibrium. The normalized island width $W/2a$ is given as a function of Θ for M/N=1/8 (1 and 2 % perturbation level) and 1/10 (2 and 4 %) helical fields.

As mentioned in the introduction, application of the nonresonant perturbation is similar to the OHTE concept in that the helical pitch is influenced in the outer region, although the applied field is much weaker than in the OHTE experiment. Since no toroidal field coil was used in OHTE, it is impossible to compare the influence of the helical fields on RFP performance. However, in view of the fact that improved performance has been observed with a perturbation level as high as ~8 % (upper bound was limited by the power supply), it may suggest the usefulness of OHTE concept. An analysis of the RFP pitch profile influenced by nonresonant perturbations is yet to be carried out.

Another possibility is the influence of external helical current on MHD instabilities. Since the applied field was externally nonresonant helical field, the corresponding modes would be external kink modes. In particular, ideal external kink mode can be unstable in a plasma surrounded by a resistive wall even if the mode is stable with ideal wall. The modes with this nature is referred to as the resistive wall modes.

4. Influence of External Helical Current on Resistive Wall Mode Stability in an RFP

The stability of ideal magnetohydrodynamic (MHD) instabilities in the present reversed field pinch (RFP) experiments relies upon a close fitting ideal conducting wall. However, in fusion relevant machines, the discharge duration τ_d has to be much longer than the field penetration time of the wall τ_s. Under these circumstances, ideal modes can become unstable with a growth time of the order of τ_s, which are referred to as the resistive shell modes (RSM).

Pioneering work on the RFP operation with a resistive wall was performed in the OHTE experiment,[8] where τ_d much longer than τ_s was realized and MHD properties were studied. There followed similar experiments with resistive walls in HBTX-1C,[9),16)] Reversatron,[10)] STE-2[11)] and Extrap T2[27)] (T2 for short). In these experiments, enhancement of the magnetic fluctuations (i.e., higher nonlinear saturation amplitudes of the tearing modes) and an increase in the loop voltage associated with enhanced helicity dissipation due to the higher fluctuation level were common observations. As for the ideal modes, growth of the external kink modes was observed in the HBTX-1C[9),16)] and Reversatron[10)], while no such observations were reported either for OHTE[8)] or T2[27)]. On the other hand, in the external helical field experiments in the STE-2,[28)] a slight improvement of the discharge

characteristics was observed when externally nonresonant helical fields were applied. These results suggest that the helical winding or the external helical current might have some influence on the stability of the external kink modes.

We will analyze the stability of the external kink modes in the RFP configuration which is surrounded by both a resistive wall and an outer helical current layer. The stability of RSM with growth rate p is determined from the dispersion relation which follows from the following boundary condition at the resistive wall

$$p\tau_s = \frac{b}{b_r}\left[\frac{\partial b_r}{\partial r}\right]_{in}^{out}, \tag{8}$$

where b_r is the radial component of the perturbed magnetic field and b the wall minor radius. The jump of $\partial b_r/\partial r$ at the resistive wall, $[\partial b_r/\partial r]_{in}^{out}$, arises from the induced wall current. Note that the thin wall approximation $b_r^{out} = b_r^{in}$ has also been used in eq.(8). When the external helical current has the effect of making the jump negative which is otherwise positive, then the mode can be stabilized by the external helical current. It is shown that this is the case with the external kink modes in the RFP configuration under some assumptions. Relevance to the experiments will also be discussed.

We will treat a simple cylindrical plasma model as shown in Fig.7 with the coordinates (r,θ,z). The plasma (whose minor radius is a) is surrounded by a resistive wall with thickness δ at $r=b$, and an outer helical current layer at $r=c$. We use the thin wall approximation $\delta/b \ll 1$. The perturbed magnetic field $\mathbf{b}$ has the form

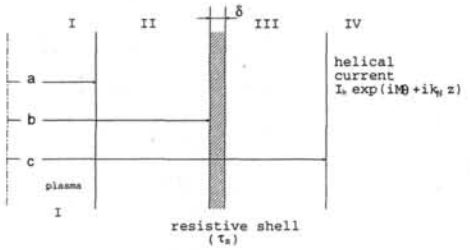

Fig.7 Cylindrical plasma model with resistive wall and outer helical current.

$$\mathbf{b} = \mathbf{b}(r)\exp(i\mathbf{k}\cdot\mathbf{r} + pt), \tag{9}$$

where $\mathbf{k} = (\mathrm{m}/r)\mathbf{e}_\theta + (\mathrm{n}/R)\mathbf{e}_z$ is the wavenumber vector with poloidal mode number m, toroidal mode number n and major radius of the simulated torus R, with the unit vectors $\mathbf{e}_\theta$ and $\mathbf{e}_z$. Hereafter we will treat only the m=1 mode because of its exclusive importance in the RFP. n/R is denoted by k_z, and capital $\mathbf{B}$ denotes the equilibrium magnetic field.

The perturbed magnetic field in the following three regions outside the plasma can be expressed in terms of the magnetic potential ϕ, which is given in each region as

region II $(a \le r \le b)$:

$$\phi_{II} = (C_1 I_r + C_2 K_r)\exp(i\theta + ik_z z + pt), \tag{10}$$

region III $(a \le r \le b)$:

$$\phi_{III} = (C_3 I_r + C_4 K_r)\exp(i\theta + ik_z z + pt), \tag{11}$$

region IV $(r \ge c)$:

$$\phi_{IV} = C_5 K_r \exp(i\theta + ik_z z + pt), \tag{12}$$

where I_r and K_r stand for $I_1(k_z r)$ and $K_1(k_z r)$, respectively and I_1 and K_1 are the modified Bessel functions.

When the growth time of the mode $1/p$ is comparable to the wall time constant τ_s, the perturbation in the plasma (region I) can be described approximately by the following marginal stability equation

$$\frac{d}{dr}(f\frac{d\xi}{dr}) - g\xi = 0, \tag{13}$$

where ξ is the radial plasma displacement and one can find the expressions for f and g elsewhere.[29]

The constants $C_j (j = 1,..., 5)$ in eqs.(10)-(12) are determined by the conventional boundary conditions at the respective boundaries. In particular, we have assumed that the phase of the helical current is matched to the component of the magnetic perturbation parallel to the wavenumber vector at $r = c$ so that the following condition holds

$$[\mathbf{k}\cdot\mathbf{b}]_{in}^{out} = \mu_0 k I_h, \tag{14}$$

where μ_0 is the magnetic permeability in vacuum and I_h the amplitude of the helical surface current density. When we neglect the curvature effect at the current layer, eq.(14) represents the jump of $\partial b_r/\partial r$ due to the helical current. It has also been assumed that the current layer is infinitely thin such that the magnetic perturbation normal to the surface is continuous at $r = c$.

We then obtain the following dispersion relation using the boundary condition given by eq.(8) at the resistive wall

$$\begin{aligned} p\tau_s &= -(1-H)\frac{bk_b^2}{k_z}\frac{K_b}{K'_b} \\ &\quad \times \frac{(\frac{I_b}{K_b} - \frac{I'_b}{K'_b})(T-1)}{\frac{I_a}{K_a} - \frac{I'_a}{K'_a} + (T-1)(\frac{I'_b}{K'_b} - \frac{I'_a}{K'_a})}, \end{aligned} \tag{15}$$

$$T = \frac{k_z}{ak_a^2}\frac{K'_a}{K_a}[(\hat{F}_a/F_a) + (r\xi'/\xi)_a], \tag{16}$$

$$H = \frac{k_z}{k_c}\frac{\mu_0 I_h}{F_a \xi_a}\frac{cK'_c}{aK_a}\frac{1}{T-1}, \tag{17}$$

where $F = \mathbf{k}\cdot\mathbf{B} = k_z B_z + (B_\theta/r)$, $\hat{F} = k_z B_z - (B_\theta/r)$, $k_a^2 = k_z^2 + (1/a^2)$ with the subscript a representing the value at $r = a$ and so on, and the prime denotes differentiation with respect to the argument.

The following force-free profile with the force-free parameter $\lambda(r)$ specified by two parameters Θ_0 and α has been adopted as a model equilibrium

$$\nabla\times\mathbf{B} = \lambda(r)\mathbf{B}, \tag{18}$$

$$\lambda(r) = (2\Theta_0/a)[1-(r/a)^\alpha]. \tag{19}$$

In Fig.8, we will give the radial profiles of the equilibrium magnetic field for three sets of the parameters Θ_0 and α. Θ_0 is the parameter associated with the central current density and α represents the peakedness of the current profile. We have neglected the plasma pressure in the present anaysis.

When there is no external helical current, we obtain the normalized growth rate vs normalized toroidal wavenumber for the equilibrium specified by four parameter sets of (Θ_0, α) as shown in Fig.9. It is essentially the same as the results in ref.9 of linear stability analysis of the external kink modes using the reduced set of MHD equations for the RFP.[30),31)] The modes with $-1.2 \leq k_z a < 0$ are unstable with the maximum growth rate at $k_z a \sim -1$, where negative n stands for the external modes. The maximum growth rate $(p\tau_s)_{max}$ is 4.0 for the equilibrium with $\Theta_0/\alpha = 1.9/3.2$, decreasing to 1.1 for 1.8/3.2, and further to 0.5 for 1.7/3.5. The external modes are more important in peaked current profile.

When there flows an external helical current with the same pitch as the mode treated, the dispersion relation shows that the mode can be marginally stable when the condition $H=1$ holds.

In Fig.10, we have plotted the helical current density (normalized to the edge radial perturbation amplitude) which is necessary to stabilize the mode with the maximum growth rate for the equilibrium specified by Θ_0 and α. Radial position of the current layer c/a is chosen as a paremeter. The figure shows that the current for stabilizing the external kink mode increases with an increase of the growth rate. The required current increases with the radial distance of the current layer; The required current is almost doubled when the current layer moves outward from $c/a=1.0$ to 1.5. It has also been confirmed that for a given value of c/a, the required current does not depend

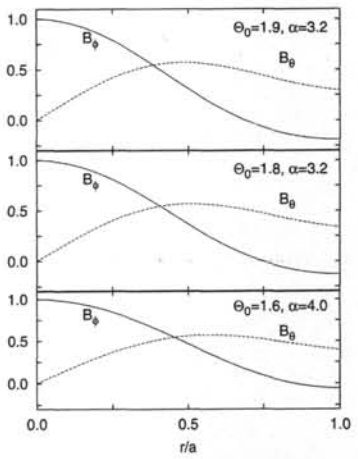

Fig.8 Radial profiles of the poloidal and toroidal magnetic fields of the model equilibria for three sets of parameters Θ_0 and α.

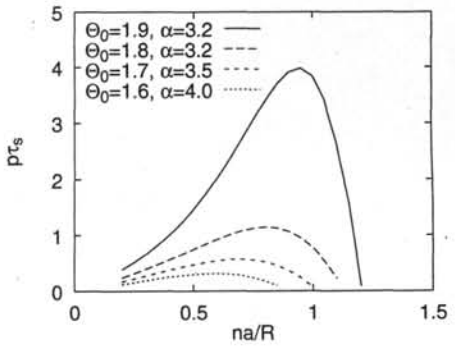

Fig.9 Normalized growth rate vs. normalized wavenumber for the equilibrium specified by four sets of Θ_0 and α.

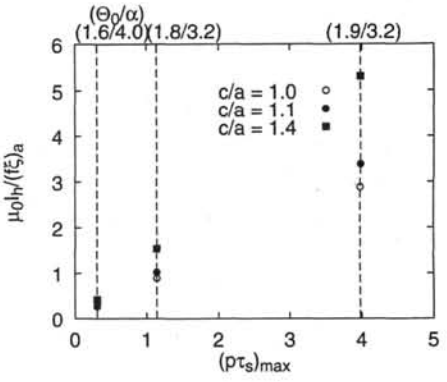

Fig.10 Helical current required to stabilize the mode with maximum growth rate for the equilibrium specified by (Θ_0/α).

strongly upon the resistive wall position b/a. In the actual situation, however, wall proximity to the plasma b/a would be determined by the requirement for ideal mode stability with a much higher growth rate. It should be noted that the normalized helical current density $\mu_0 I_h/(f\xi)_a$ can be rewritten as $(2\pi a I_h/I_p)/(|\tilde{B}_{ra}|/B_{\theta a})$, where I_p is the plasma current and $|B_{ra}|$ the radial magnetic fluctuation amplitude. Since the radial magnetic fluctuation level $|\tilde{B}_{ra}|/B_{\theta a}$ is several % in the experiments, Fig. 10 suggests that the total helical current of less than 10 % of the plasma current is enough to stabilize the external kink modes.

As mentioned in the beginning of this section, in the resistive wall RFP experiments to date, they observed growth of the external kink modes in some machines while they did not in others. Since the external kink mode stability depends on the current profile as shown in Fig.9, we may be able to attribute the difference to the current profiles in different devices. We should note, however, that there appears to be no significant difference of the pinch parameter Θ $(=B_{\theta a}/<B_z>)$ and field reversal ratio $F(=B_{za}/<B_z>)$ in these experiments, where the bracket <> denotes the corss sectional average.

A possible alternative interpretation is the effect of the external helical current induced in the external structure whose decay time constant is longer than the resistive wall time constant. As shown in the present analysis, the induced helical current would have a stabilizing effect on the external kink modes if the phase of the induced current coincides with that of the component of the magnetic perturbation parallel to the wavenomber vector. It may be interesting to note that both OHTE and T2 are equipped with external helical windings.

In STE-2,[28] as shown in the previous section, a slight improvement of an RFP discharge was observed with externally nonresonant helical fields. In the experiments, helical perturbations with M/N=1/-8 and 1/-10 were applied, where M and N are the poloidal and toroidal mode numbers of the external fields, respectively. The toroidal mode number spectrum in the experiments would probably not be very narrow because of the inevitable toroidally nonuniform pitch of the helical windings and winging "error", both at the diagnostic ports and at the support structures of the windings. Non-negligible amplitude may thus be distributed to the N~-4 component (which is also subharmonic of the M/N= 1/-8 field) in the applied helical field. We can therefore put forth that one of the possible mechanisms of the slight improvement of the RFP with an externally nonresonant helical field is the stabilizing effect of the external current on the external kink modes. Unfortunately, magnetic diagnostics were insufficient to identify the toroidal mode numbers of the instabilities in those experiments. Similar experiments are under way with improved magnetic diagnostics.

In the experiments with much longer discharge duration, feedback control[16] of the helical current (field) would be needed by the use of two pairs of helical coils with are orthogonal to each other. Since the spectrum of toroidal mode numbers of the unstable external kink modes is rather narrow, lying in the range $1 \leq |n| \leq R/a$ as shown in Fig.8, it may not be very difficult to stabilize these modes with feedback control technique.

5. Control of Mode Dynamics with Rotating Helical Field

As mentioned in the previous section, the resistive wall modes (RWM) (both tearing and ideal kink modes) are thought to be serious problems in future RFPs in which the discharge duration far exceeds the field penetration time of a conducting wall. Theories have predicted that the growth of tearing modes or their saturation amplitudes can be reduced by moderate toroidal rotation of the plasma.[30] On the other hand, stabilization of the external kink modes requires sub Alfvénic rotation speed which is much faster than the natural rotation speed of the tearing modes.[32]

In the RFP, it appears to be difficult to use the neutral beam injection for plasma rotation drive because the diameter of port holes is restricted by the unfavorable field errors. Thus, development of other techniques for rotation drive is one of the urgent issues in the RFP research. The internally resonant rotating helical field (RHF) applied from outside of the resistive wall may be able to provide accelerating torque to the magnetic island, if the phase is adequately controlled. The external kink modes may be stabilized by externally nonresonant rotating helical field which resembles the rotating secondary shell concept.[33]

In the preliminary experiments,[34] we used helical coils covering a half of the torus (two quarters), which provided M/N=1/8 resonant RHF. The discreteness of the helical coil produced the low N (~2) components of the M=1 field as well. No significant influence of the RHF was observed on the m=1 mode dynamics. However, toroidally localized m=0 (toroidal flux) disturbance was accelerated or decelerated depending upon the direction of the RHF. This result may indicate that the m=0 disturbance was a result of the m=1 mode coupling.

In this section, we describe the results which indicate direct interaction between the rotating M=1 helical field and the inherent m=1 core resonant tearing modes. The helical coils have been modified to cover the whole torus, which has resulted in a rather sharp toroidal mode spectrum of the RHF; the amplitudes of the M/N=1/7,9 components are about a half of that of the main M/N=1/8 component, while the rest is negligibly small. In most experiments reported here we used LC damping oscillation to obtain alternating current; effective duration of the rotating field was restricted to not longer than 0.3-0.4ms. The frequency was 10-20kHz, and the toroidal phase velocity of the RHF was 4-7 km/s. The amplitude of the oscillating field $|B_{ra}|$ is defined as an average from the second to the fifth peak values which were measured inside the vessel.

In STE-2 discharges without a conducting shell, the plasma current I_p is around 60 kA with discharge duration τ_d of around 0.7 ms.[34] Figure 11 shows the time behavior of the m=1 edge radial magnetic fluctuations $\tilde{B}_{ra}$ measured with a toroidal

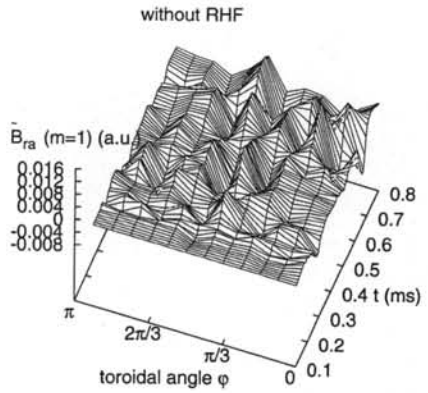

Fig.11 Time evolution of $\tilde{B}_{ra}$ over a half of the torus without RHF.

array of sine/cosine coils attached onto the outer surface of the vacuum vessel and covering over a half of the torus. Immediately after attaining the RFP configuration at about $t=0.25$ ms, the magnetic fluctuations grow with the time scale of τ_w, and the dominant toroidal mode number n appears to be around 8, maintaining the structure for the rest of discharge. The fluctuations remain almost nonrotating (i.e., locked to the vessel). The measurement of radial magnetic field profile shows that the m/n=1/8 mode is the tearing mode whose resonant surface is located at $r/a\sim0.4$.

When the RHF was applied at 0.3 ms with a frequency of 15 kHz and a perturbation level of 0.5 %, as shown in Fig.12, the amplitude of magnetic fluctuations is reduced, and, furthermore, the fluctuations rotate toroidally in the direction of the applied RHF. The phase velocity of magnetic fluctuations is slightly lower than that of the RHF. It should be noted that there is a critical perturbation amplitude; When the perturbation level is lower than 0.4 %, which almost coincides with the edge flucutation level of intrinsic mode, neither the reduction of the fluctuation amplitude nor their toroidal rotation has been observed.

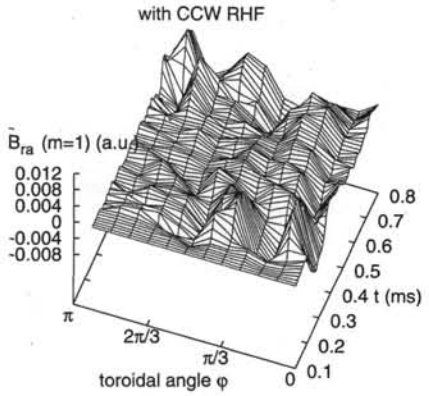

Fig.12 Time evolution of $\tilde{B}_{ra}$ with RHF applied at 0.3 ms.

The toroidal mode spectrum of the $\tilde{B}_{ra}$ shows that most of the fluctuation power is distributed among the m/n=1/7,8,9 modes. Figure 13 shows the time evolution of the amplitudes of these m/n=1/7,8,9 modes together with the plasma current waveform without the RHF. The amplitudes of the modes increase immediately after setting up the RFP configuration with the time scale of the vacuum vessel until the end of discharge. When the RHF is applied at 0.3 ms with relative amplitude of 0.5 %, the time evolution of the mode amplitudes changes, as shown in Fig.14. The growth of the modes is suppressed transiently for 0.2-0.3 ms, and, moreover, the amplitudes are reduced for the rest of the discharge. Ensemble average over several tens of shots has revealed that the amplitudes of these modes are reduced by 20-30 % at 0.5 ms.

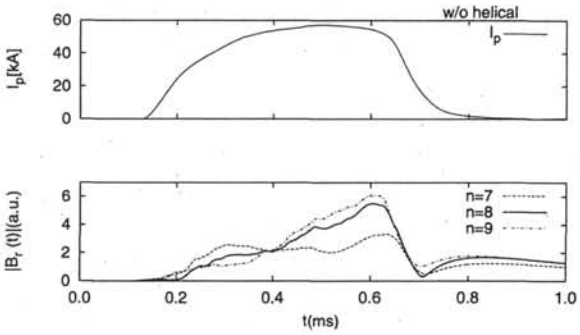

Fig.13 Time evolution of the m/n=1/7,8,9 mode amplitudes without RHF.

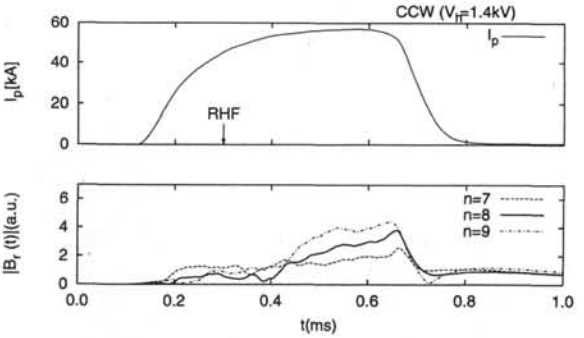

Fig.14 Time evolution of the m/n=1/7,8,9 mode amplitudes with RHF applied at 0.3 ms.

The time behavior of the toroidal phases of the m/n=1/6-10 modes shows

that the core resonant (or internally nonresonant) m/n=1/≤8 modes are almost locked to the vessel, while the m/n=1/9,10 modes rotate in the opposite direction to the toroidal plasma current (ctr-direction) with a phase velocity of $\sim 5\times10^3\pi$rad/s. It may be interesting to note that in the ultra-low-q (ULQ) discharges in the STE-2, the dominant m/n=1/5-7 modes rotate rigidly in the same (ctr-) direction with almost the same phase velocity. When the RHF is applied at 0.3 ms, as shown in Fig.15, the m=1/n=8 mode keeps moving (or rotates) for ≥0.2 ms, and at the same time, the m/n=1/9 mode, which otherwise ctr-rotates, reverses the rotation direction and keeps moving for the same period. The m/n=1/10 mode may also be decelerated for the remaining period of the discharge. Further discussion on the behavior of these m=1 modes, which probably includes the effect of resonant three wave coupling through nonlinearly excited m=1/low n modes, requires simultaneous measurements of the m=1 and m=0 modes. Nevertheless, we may conclude that the above result is the first demonstration in the RFP of the direct interaction between the rotating M=1 helical field and inherent m=1 core resonant tearing modes.

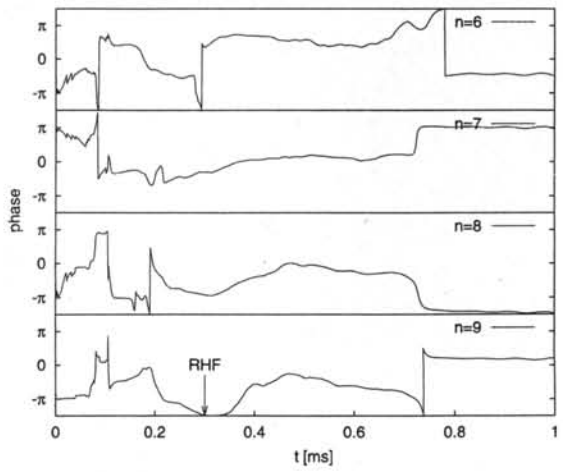

Fig.15 Time evolution of the toroidal phase of the m/n=1/6,7,8,9 modes with RHF applied at 0.3 ms.

In the present experiments with improved helical coil configuration, it has also been observed that the toroidally localized m=0 disturbance, which usually rotates in the ctr-direction, is either accelerated or decelerated depending upon the RHF direction, as in the previous experiments. The influence of the M=1 RHF on the toroidal rotation of the m=0 localized disturbance has also been identified

Figure 16 shows the resistance vs. toroidal plasma current in standard and RHF-applied discharges. The resistance decreases with an increase in the plasma current in both cases. No significant improvement of the dependence of the resistance on plasma current has not been made clear yet. However, it may be noted that the plasma current tends to increase with the RHF. Influence of the RHF on high frequency magnetic fluctuations has not been observed yet. Further optimization of both the frequency (rotation speed) and amplitude of the RHF is in progress with the use of a pair of pulsed oscillators with helical current $I_h < 1$ kA in the frequency range of 10 kHz $< f <$ 30 kHz.

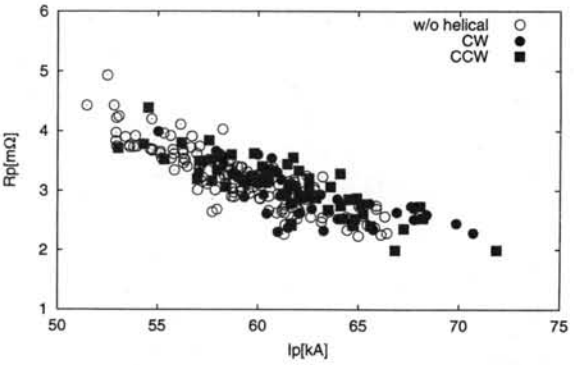

Fig.16 RFP discharge resistance vs. plasma current in standard and RHF-applied discharges.

Some theories have been proposed very recently[36),37)] on the interaction of inherent

tearing mode with external rotating helical field in the RFP configuration. Stability boundaries have been obtained in the amplitude vs. frequency space of the rotating field. Comparison with this theory is inevitable for further quantitative discussion.

6. Summary

Response of an RFP plasma to external static helical perturbations has been found to depend upon the helicity of perturbation.

Degradation of discharges has been observed with resonant perturbations, being characterized by higher discharge resistance and shorter RFP lifetime. In the degrared discharges, edge magnetic fluctuation level increases with some indications of enhanced coupling of both m=1 and m=0 modes; The coherence scale length decreases with increased fluctuation level and localized toroidal flux disturbance grows near the poloidal gap. Critical perturbation level of M/N=1/8 field for sufficient degradation is lower than that of M/N=1/10 field by a factor of about 2.

Analysis of the static island width in M=1 helically perturbed RFP equilibria shows that the above critical level corresponds to production of the static magnetic island with the width comparable to the radial distance to the neighboring rational surfaces. The factor 2 difference of the critical peturbation level depending on the perturbation helicity roughly agrees with the calculation. The enhanced m=1 mode coupling with application of the resonant perturbation thus results from interaction between the static and inherent islands the latter being associated with m=1 tearing modes.

RFP discharges are improved slightly with application of the nonresonant perturbations. In these improved discharges, the fluctuation level and coherence scale lenght do not change appreciablly, while toroidal uniformity of the toroidal magnetic flux has been improved significantly, which is an indication of the suppression of the m=0 mode coupling. The $F-\Theta$ loci implies slight suppression of the m=1 mode coupling, however, no direct evidence has not been obtained.

A stability analysis of the ideal external kink mode has been performed in an RFP surrounded by a resistive wall and an outer helical current. The helical current is shown to have a stabilizing effect on this particular mode. Thus, the external helical current is one of the possible mechanisms for the improvement. Further experimental efforts are to be made to identify the external kink mode.

The STE-2 RFP has been operated with only a vacuum vessel to test the idea of driving the mode and/or plasma rotation using resonant RHF applied from outside of the vessel. It has been observed that the growth of dominant magnetic fluctuations, which are otherwise almost locked to the vessel, is suppressed with transient rotation. It is a direct demonstration of the interaction between the externally applied M=1 modes and the inherent core resonant tearing modes.

The external helical field appears to be useful in controlling the RFP dynamics.

Acknowledgment

The authors thank K. Ohta for his technical assistance. They are also grateful to Professor T. Tamano, Professor M. Wakatani, Dr. Y. Hirano, Dr. Y. Yagi, Progessor S. Prager, Dr. J. Sarff, Dr. C. Hegna, Dr. S. Ortolani for useful discussions.

Department of Electronics and Information Science
Faculty of Engineering and Design
Kyoto Institute of Technology
Matsugasaki, Sakyo-ku, Kyoto 606-8585

References

1) J.B. Taylor, *Rev. Mod. Phys.* **58**, 741 (1986).
2) S. Ortolani and D.D. Schnack, "Magnetohydrodynamics of Plasma Relaxation", World Scientific, Singapore (1993).
3) M.R. Stoneking, S.A. Hokin, S.C. Prager et al., *Phys. Rev. Lett.* **73**, 549 (1994).
4) G. Fiksel, S.C. Prager, W. Shen and M.R. Stoneking, *Phys. Rev. Lett.* **72**, 1028 (1994).
5) J.S. Sarff, N.E. Lanier, S.C. Prager and M.R. Stoneking, *Phys. Rev. Lett.* **78**, 62 (1997).
6) Y. Hirano, Y. Maejima, T. Shimada et al., *Nucl. Fusion* **36**, 721 (1996).
7) T. Tamano, W.D. Bard, W.D. Chu et al., *Phys. Rev. Lett.* **59**, 1444 (1987).
8) R.J. La Haye, P.S. Lee, M.J. Schaffer et al., *Nucl. Fusion* **28**, 918 (1988).
9) B. Alper B, M.K. Bevir, H.A.B. Bodin et al., *Plasma Phys. Control. Fusion* **31**, 205 (1989).
10) P. Greene and S. Robertson, *Phys. Fluids B* **5**, 556 (1993).
11) S. Masamune, K. Kawasaki, A. Mutara et al., *Plasma Phys. Control. Fusion* **35**, 209 (1993).
12) J.R. Drake, H. Bergsaker, R.R. Brunsell et al., "Fusion Energy 1996", IAEA, Vienna (1997).
13) C.G. Gimblett, *Nucl. Fusion* **26**, 617 (1986).
14) Z.X. Jiang, A. Bondeson and R. Paccagnella, *Phys. Plasmas* **2**, 442 (1995).
15) E.J. Zita, S.C. Prager, Y.L. Ho and D.D. Schnack, *Nucl. Fusion* **32**, 1941 (1992).
16) B. Alper, *Phys. Fluids B* **2**, 1338 (1990).
17) R. Fitzpatrick, *Nucl. Fusion* **33**, 1049 (1993).
18) D.J. Den Hartog, A.F. Almagri, J.T. Chapman et al., *Phys. Plasmas* **2**, 2281 (1995).
19) T. Ohkawa, M. Chu, C. Chu and M. Schaffer, *Nucl. Fusion* **20**, 1464 (1980).
20) R.J. La Haye, T.N. Carlstrom, R.R. Goforth et al., *Phys. Fluids* **27**, 2576 (1984).
21) S. Masamune, M. Iida, N. Oda et al., "Fusion Energy 1996", IAEA, Vienna (1997).
22) S. Masamune, M. Iida, D. Ishijima et al., *Fusion Technology* **27**, 293 (1994).
23) Y.L. Ho and S.C. Prager, *Phys. Fluids B* **3**, 3099 (1991).
24) S. Assadi S, Ph D Thesis, University of Wisconsin, DOE/ER/53198-234 (1994).
25) S. Masamune, K. Iida M, Ohta and H. Oshiyama, *J. Phys. Soc. Jpn.* **67**, 2977 (1998).
26) R.I. Pinsker and A.H. Reiman, *Phys. Fluids* **29**, 782 (1986).
27) G. Hedin, *Plasma Phys. Control. Fusion* **40**, 1529 (1998).
28) S. Masamune, M. Iida, Y. Ohfuji et al., *Plasma Phys. Control. Fusion* **40**, 127 (1998).
29) K. Miyamoto, "Plasma Physics for Nuclear Fusion (2nd ed.)", MIT Press, Cambridge (1989); J.P. Freidberg, "Ideal Magnetohydrodynamics", Plenum Press, New York (1987).
30) T.C. Hender, C.G. Gimblett and D.C. Robinson, *Nucl. Fusion* **29**, 1279 (1989).
31) H.R. Strauss, *Phys. Fluids* **27**, 2580 (1984).
32) S.C. Guo et al., *Phys. Plasmas* **6**, 3868 (1999).
33) C.G. Gimblett, *Plasma Phys. Control. Fusion* **31**, 2183 (1989).
34) S. Masamune, M. Iida et al., "Fusion Energy 1998", IAEA, Vienna **3**, 919 (1999).
35) S. Masamune, M. Iida and H. Oshiyama, *J. Phys. Soc. Jpn.* **68**, 2161 (1999).

36) S.C. Guo and M.S. Chu, *Phys. Plasmas* **7**, 3342 (2001).
37) R. Fitzpatrick and P. Zanca, "Phase-locking of tearing modes in reversed field pinch plasmas", preprint, Institute of Fusion Studies, University of Texas at Austin (August 2001).